Proceedings: Fifth International Conference on Case Histories in Geotechnical Engineering
New York, NY, April 13-17, 2004

FOUNDATION OPTIMIZATION AND DESIGN FOR REPLACEMENT OF THE WOODROW WILSON BRIDGE

Theme No. 9

Roderic A. Ellman, Jr., PE
Mueser Rutledge Consulting Engineers
New York, NY (USA)

Sissy Nikolaou, PhD
Mueser Rutledge Consulting Engineers
New York, NY (USA)

Mishac K. Yegian, PhD, PE
Northeastern University
Boston, MA (USA)

ABSTRACT

The new Woodrow Wilson Bridge (WWB) will replace the existing bridge over the Potomac River to connect Alexandria, Virginia to Prince Georges County, Maryland. The new WWB will extend approximately 1.1 miles across the river, with a 367-ft long bascule span in the main river channel where the water depth is about 36 ft. The subsurface soil profile consists of up to 50 ft of a soft organic silty clay layer that is very vulnerable to scour, underlain by a deep deposit of hard sandy clay.

This paper will present results from a Pile Demonstration Program (PDP) that was conducted as part of the bridge replacement project, discuss the various aspects of the seismic design and analysis, and describe how those data were applied to optimize foundation design. The PDP included dynamic monitoring, static load tests and Statnamic load tests at several locations, to evaluate: (i) the pile driveability and associated parameters necessary for dynamic analysis; and (ii) the ultimate skin friction and end bearing values for design. The PDP provided a basis for eliminating static load tests during construction and construction quality control, and for evaluating potential settlement of the existing bridge. Although the seismicity of the region is low, considering the importance of this bridge and the consequences of potential damage during an earthquake, seismic issues were addressed thoroughly in the design of the new structure, including: (i) development of design spectra based on site-specific seismic hazard and ground motion analyses; (ii) implications of the complex soil profile and potential scour on the dynamic response of the foundations; (iii) Soil-Structure Interaction (SSI) analyses for the various foundation alternatives; and (iv) evaluation of the significance of the kinematic SSI effect on the piles.

The presented case study proves how results of a pile demonstration program and extensive seismic studies can enable significant optimization of the foundation design and cost savings, and provide significant quality control during construction.

INTRODUCTION

The Woodrow Wilson Memorial Bridge is the only Potomac River crossing in the southern half of the Washington Metropolitan area (Fig. 1) to connect Alexandria, Virginia to Prince Georges County, Maryland.

Consisting of fixed spans and a movable (bascule) span, it carries the Capital Beltway (I-495), which is part of I-95, the main north-south interstate route on the East Coast. Approximately 1.1-mile long, a new bridge has been designed for HS25 loads consisting of six lanes for local traffic, four lanes for express traffic, and two HOV lanes. Provisions are made for future replacement of the HOV lanes with rail. The bascule span is 367-ft long in the main river channel where the water depth is about 36 ft, with 174 ft wide navigation channel. In 1998, Maryland State Highway Administration awarded Parsons Transportation Group (PTG) the design and construction support services of the new bridge. Mueser Rutledge Consulting Engineers (MRCE) performed the foundation design.

An arch-like appearance has been achieved by introducing V-shaped piers with curved legs, which support haunched girders (Fig. 2). This structural system consists of independent structural units (V-piers), and produces zero horizontal thrust forces under dead and live loads. The subsurface soil profile consists of up to 50 ft of a soft organic silty clay layer that is very vulnerable to scour, underlain by a deep deposit of hard sandy clay. Proper arrangement of the girder spans balances

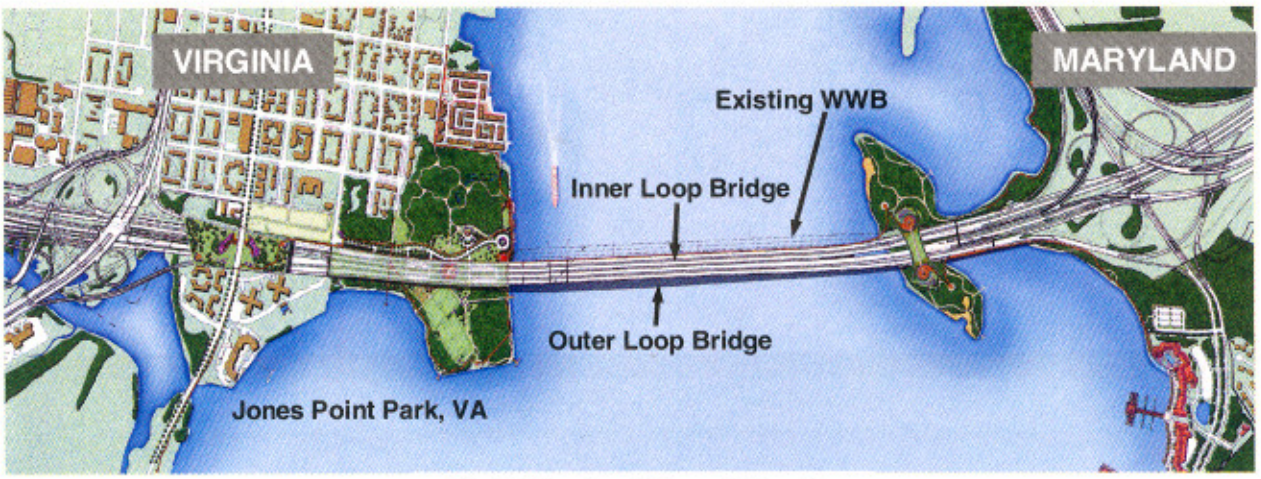

Fig. 1. Woodrow Wilson Bridge site.

the dead loads and produces minimal bending moments at the piers. This system eliminates the need of using batter piles and results in significant savings in the foundations, especially at the bascule piers located in the deepest part of the river.

In order to optimize the pile design it is generally most effective to maximize the load carrying capacity of the piles that usually results in larger pile cross section and deeper penetration. Equally important in the optimization process is the consideration of pile installation issues namely, fabrication, lifting and handling, splicing and driveability.

PILE DEMOSTRATION PROGRAM

A Pile Demonstration Program (PDP) during the design phase was undertaken between April and July 2000 to evaluate the driving and load carrying performance of piles for the new bridge. The program included three load test locations as shown in Fig. 3. Location PL-1 was in the river between Outer Loop Piers M1 and M2; Location PL-2 was in the river between Outer Loop Piers M8 and M9; and Location PL-3 was on land between Inner Loop Piers V3 and V4. Tests on open-ended steel pipe piles included three 54″ diameter by 1″ wall, (piles A, B and C) at PL-1 installed with an IHC S-280

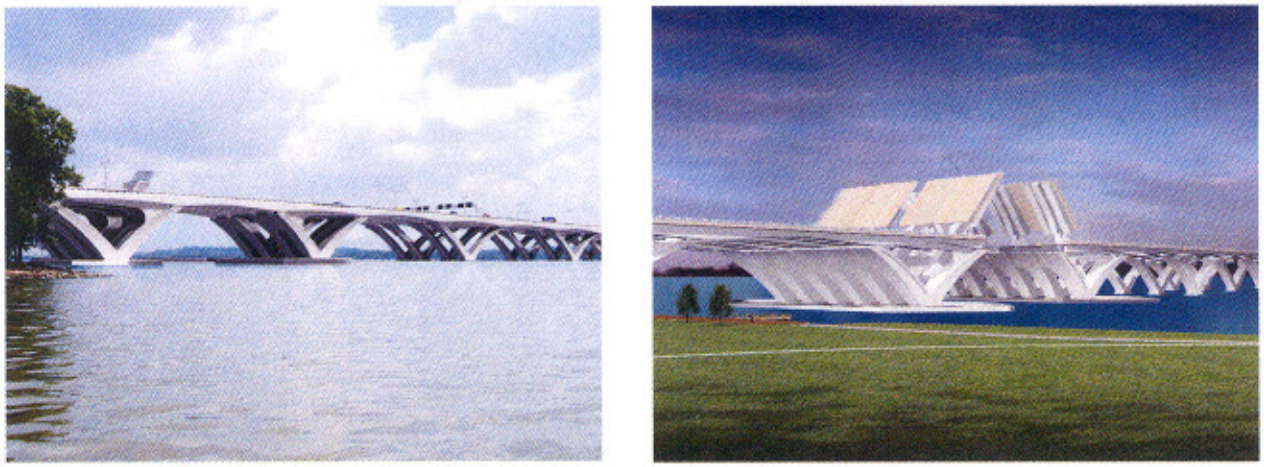

Fig. 2. Computer generated photographs of the new Woodrow Wilson Bridge.

This paper will present two basic aspects of the foundation analysis and design: (a) the extensive Pile Demonstration Program (PDP) and (b) the seismic Soil-Structure Interaction (SSI) effects. This case study will show how results of the PDP program and extensive earthquake studies enabled significant optimization of the foundation design and cost savings, and provided a means for quality control during construction.

hydraulic hammer with rated energy of 206 ft. kips; three 42″ diameter by 1″ wall piles at PL-2 (piles D, E and F) also installed with the IHC S-280 hydraulic hammer, and one 36″ diameter by 1″ wall pile (pile I) at PL-3 installed with an ICE-275 hydraulic hammer with rated energy of 110 ft. kips. Two 24″ square, precast, prestressed concrete piles (piles G and H) were also installed with the ICE-275 hammer at PL-3. The piles were fitted with either electrical resistance or vibrating wire strain gages spaced along the length of the piles.

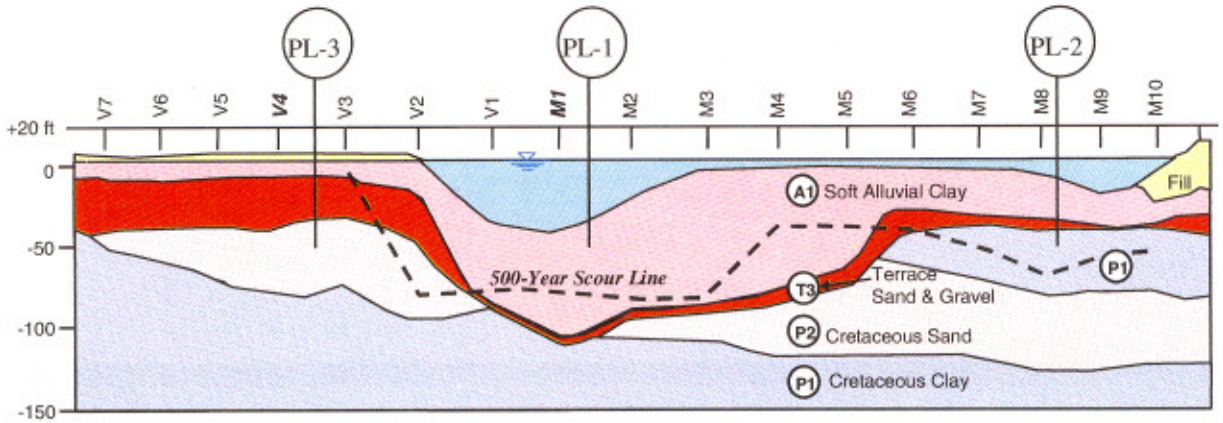

Fig. 3. Soil and estimated scour profile, bridge pier locations, and pile load test locations.

The load test program included initial driving with PDA monitoring followed by 7-day and/or 14-restrike. The data from selected blows were analyzed using CAPWAP. Static axial load tests were performed at piles C, F, G and I, in accordance with ASTM D-1143.

Table 1 summarizes pile load test results including: test location and hammer used, pile number, pile size, pile tip elevation, bearing stratum, initial driving performance, 7-day and 14-day restrike performance; CAPWAP analyses including shaft resistance, skin quake, skin damping, toe resistance, toe quake, toe damping and total capacity; and load test data including static failure load and corresponding average skin friction, and Statnamic mobilized load and corresponding average skin friction.

Generally, all piles experienced light to moderate driving resistance. Driving stresses for the steel piles ranged between 20 and 35 ksi which is within the allowable prescribed by AASHTO for grade 50 steel. Driving stresses for the concrete piles ranged between 1.7 to 3.3 ksi compression and between 0.13 to 0.5 ksi tension, also within allowable values prescribed by AASHTO for 5,000-psi prestressed concrete piles.

Table 1. Summary of pile demonstration program.

PILE LOAD TEST LOCATION (HAMMER)	PILE No.	PILE SIZE	PILE TIP ELEV.	BEARING STRATUM	INITIAL DRIVING PERFORMANCE		7-DAY RESTRIKE PERFORMANCE		14-DAY RESTRIKE PERFORMANCE		CAPWAP ANALYSES							LOAD TEST DATA AXIAL				LATERAL
					DRIVING RESIST. (bl/ft)	PDA CAPACITY (kips)	DRIVING RESIST. (bl/ft)	PDA CAPACITY (kips)	DRIVING RESIST. (bl/ft)	PDA CAPACITY (kips)	SHAFT CAPACITY (kips)	QUAKE SKIN (in)	DAMPING SKIN (sec/ft)	TOE CAPACITY (kips)	QUAKE TOE (in)	DAMPING TOE (sec/ft)	TOTAL CAPACITY (kips)	STATIC FAILURE (kips)	AVERAGE SKIN FRICT. (ksf)	STATNAMIC MOB. LOAD (kips)	AVERAGE SKIN FRICT. (ksf)	STATIC FAILURE (kips)
PL-1 (IHC S-280)	A	54" x 1"	-158	P1 Clay	50	2760					2734	0.100	0.135	26	0.513	0.115	2760					
	A	54" x 1"	-158	P1 Clay						3410	3610	0.077	NA	584	0.239	NA	4194					
	A	54" x 1"	-195	P1 Clay	120	not measured																
	B	54" x 1"	-153	P1 Clay	40	2660					2264	0.094	0.120	386	0.398	0.112	2650					
	B	54" x 1"	-153	P1 Clay	40	2660			6	3140	3600	0.101	0.120	650	0.243	0.115	4250			5300	3.4	
	C	54" x 1"	-157	P1 Clay	49	2430					2985	0.097	NA	148	0.241	NA	3133	2929	1.7			
PL-2 (IHC S-280)	D	42" x 1"	-105	P2 Sand	42	2110					2074	0.100	0.120	207	0.479	0.074	2281					
	D	42" x 1"	-112	P2 Sand					11	2680	2088	0.100	NA	472	0.307	NA	2560					
	E	42" x 1"	-112	P2 Sand	40	1850	6	2600		2920	2316	0.100	0.120	23	0.579	0.115	2339					
	E	42" x 1"	-112	P2 Sand			6	2600		2920	1188	0.100	NA	1136	0.307	NA	2324					
	E	42" x 1"	-112	P2 Sand						2920	2654	0.100	NA	294	0.010	NA	2948			4360	4.9	
	F	42" x 1"	-118	P2 Sand	40	1960	6	2700			1546	0.100	0.200	143	0.512	0.200	1689					
	F	42" x 1"	-118	P2 Sand			6	2730			2493	0.100	NA	293	0.263	NA	2786	>2000	2			
PL-3 (ICE - 275)	G	24" x 24"	-33	P2 Sand		980					291	0.100	0.180	836	0.537	0.137	1127					
	G	24" x 24"	-33	P2 Sand				940			130	0.100	NA	781	0.400	NA	911					
	G	24" x 24"	-33	P2 Sand						890	166	0.122	NA	730	0.400	NA	896					
	G	24" x 24"	-44	P2 Sand	80	1190					218	0.100	0.200	1080	0.487	0.106	1298					
	H	24" x 24"	-44	P2 Sand	60	1250					128	0.097	NA	1110	0.477	NA	1238					
	H	24" x 24"	-44	P2 Sand			40/6"	1420			514	0.097	NA	797	0.272	NA	1311					
	H	24" x 24"	-44	P2 Sand					50/6"	1400	593	0.100	NA	731	0.242	NA	1324	>1900				55
	I	36" x 1"	-84	P1 Clay	38	1450					1092	0.105	NA	119	0.296	NA	1211					
	I	36" x 1"	-84	P1 Clay			7	1710			1232	0.100	NA	145	0.350	NA	1377					
	I	36" x 1"	-84	P1 Clay					6	2210	1764	0.097	NA	17	0.166	NA	1781	1650	2			55

The Statnamic tests gave significantly greater pile capacities and unit skin frictions than measured by PDA, calculated by CAPWAP, or as determined by conventional static load tests. There is poor correlation between static pile capacity and Statnamic capacity. Therefore, static test results were used to provide the basis for assessing the load capacity of the piles.

SOIL RESISTANCE TO DRIVING

Open-Ended Steel Pipe Piles

Our assessment of driveability for the open-end steel pipe piles began with the initial driving data obtained from monitoring 54" piles A, B, and C at location PL-1 in the central river channel. The soil profile at PL-1 is representative with regard to deep pile penetration at the proposed bridge, being underlain by P1 clays below El -100. Figure 4 shows the increase in soil resistance during initial driving as indicated by the PDA results and by CAPWAP analysis. The CAPWAP data conform particularly well to a linear increase with depth. Both data sets indicate an average increase in soil resistance during initial driving of about 38 kips per ft.

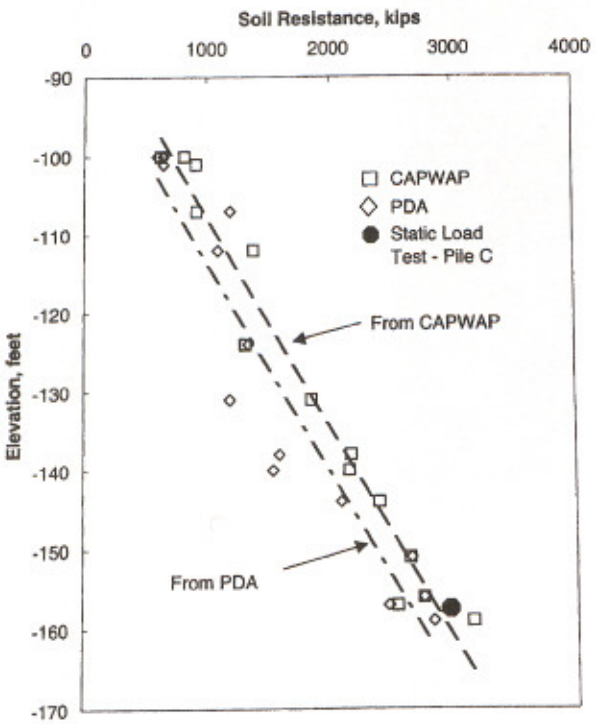

Fig. 4. Soil resistance during initial driving at location PL-1 for 54" pipe piles A, B, and C.

Measurements indicated that the open-end pipe piles did not plug during driving. The relative proportion of skin friction that acted on the outside and inside of the pile wall is unknown. Normal practice in the offshore industry is to assume that zero skin friction acts on the inside of the pile in soft clays (Dutt and Collins, 1995). For stiff clays, the inside skin friction is taken as 50 to 100% of the outside friction (Stevens et al, 1982). Having deduced the shaft load transfer, it actually does not matter whether the resistance is assumed to act on the outside and/or inside of the pile wall, only that a consistent approach is taken to back analysis and prediction.

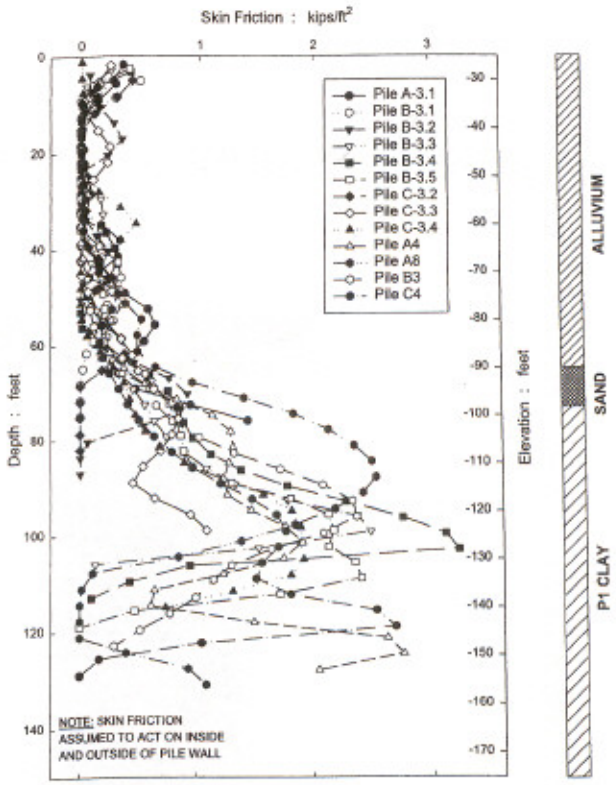

Fig. 5. Skin friction during driving at location PL-1.

To avoid confusion, the simple assumption can be made that, for these "coring" piles, the inside and outside skin friction are the same. The increase in soil resistance of 38 k/ft, obtained from Fig. 4, corresponds to a unit skin friction of about 1.35 ksf acting on the inside and outside of the pile wall. This value applies to the P1 clay between El -100 and -160, the maximum penetration for which such data are available. The corresponding skin friction distributions obtained from CAPWAP analysis for initial driving at PL-1 are summarized on Fig. 5.

The overall pattern of skin friction conforms to expectations in that the resistance in the alluvium is quite limited, and increases when the stronger underlying soils are encountered. There is, however, significant variability in the CAPWAP computed skin friction in the P1 clay, both along the length of the pile and from case to case. This variation undermines confidence in the information, which is obtained from a theoretical analysis of measured data. The analysis depends on a number of assumptions, and is particularly uncertain for open-end pipe piles. In an attempt to counter the variability in skin friction distribution, the average profile of Fig. 6 was developed from the information on Fig. 5.

Based on the information on Figs 4 to 6, values judged to be representative were chosen for skin friction in the alluvium (0.25 ksf) and for the underlying stronger soils (1.25 ksf). As discussed below, these values were used in wave equation analyses to obtain blow counts for comparison with the observed pile driving. The values of skin friction for the weak-over-strong soil profile could be refined so that the computed blow counts matched the observed blow counts. The process developed from the 54″ pile monitoring data at location PL-1 was then repeated for the 42″ and 36″ pipe piles at locations PL-2 and PL-3. Observations indicated that the piles did not plug during driving and that end bearing was a small component of the total driving resistance.

Precast Prestressed Concrete Piles

24″ square concrete piles G and H were installed using the ICE-275 hydraulic hammer with rated energy of 110 ft-kips. Pile G was initially driven to El -33 with a final driving resistance of 40 bpf corresponding to soil resistance of 980 kips by PDA. Pile G was re-driven to tip El -44 (final driving resistance of 80 bpf, soil resistance of 1190 kip by PDA). Pile H was installed to El -44 with a final driving resistance of 60 bpf corresponding to a soil resistance of 1200 kips by PDA. CAPWAP analyses indicated that the soil resistance acting on the concrete piles was equally distributed between shaft and tip, with a total capacity of 1300 kips.

WAVE EQUATION ANALYSIS

Input Parameters

Wave equation analysis requires a number of inputs in addition to pile and hammer type, including hammer efficiency and parameters to define the static and dynamic resistance of the soil. The 54″ and 42″ pipe piles were driven with an IHC model S-280 hammer having a maximum rated energy of 206 ft-kips. The 36″ pipe piles were driven with an ICE model 275 hammer having a maximum rated energy of 110 ft-kips. Referring to Table 1, the cases selected for calibrating the driveability prediction procedure were Pile A (El -158 and -195), Pile D (El -105), Pile F (El -118), and Pile I (El -84). Monitoring data indicate that the IHC S-280 hammer transferred between 170 and 200 ft-kips of energy, while the ICE 275 transferred about 90 ft-kips of energy to the pile. We used a hammer efficiency of 90 to 95% for hydraulic hammers, which resulted in transfer energies of 190 and 100 ft-kips for the IHC S-280 and ICE-275, respectively. These values are on the high side of the observations, however the difference is moderated by the relative insensitivity of driveability to small changes in hammer energy.

The soil quake and damping parameters were obtained from the results of CAPWAP analyses (Table 1). The wave equation analyses performed for the piles indicate that the observed driving behavior can be recaptured using a single set of parameters for the site. The static skin friction was also based on the CAPWAP analyses (Figs 1 to 3). The parameters used in this assessment are given in Table 2.

Table 2. Wave equation analysis parameters.

Parameter	Value	Parameter	Value
Skin Friction in Fill and Alluvium	0.25 ksf	Side and Tip Damping	0.12 sec/ft
Skin Friction in P1 Clay and P2 Sand	1.25 ksf	Side Quake in Sand and Clay	0.1"
End Bearing in Clay	60 ksf	Tip Quake in Clay	0.3"
End Bearing in Sand	180 ksf	Tip Quake in Sand	0.5"

The piles are considered to core the soil without formation of an internal soil plug. The skin friction values apply to both the internal and external surfaces of the pile wall. The end bearing values apply to the steel annulus area of the pile. Analysis for a coring 54″ pile with the tip at El -158 used skin friction values of 0.25 and 1.25 ksf for the "weak-over-strong" profile, with the top of the weak and strong soils at El -27 and El.-90, respectively. The analysis indicated a driving resistance of 50 bpf, which was in accordance with field observations (Table 1). The skin friction values of 0.25 and 1.25 ksf for the weak-over-strong profile were then used to predict the blow count for the same pile at El -195 (Fig. 6). A satisfactory match was obtained (130 vs. 120 bpf observed).

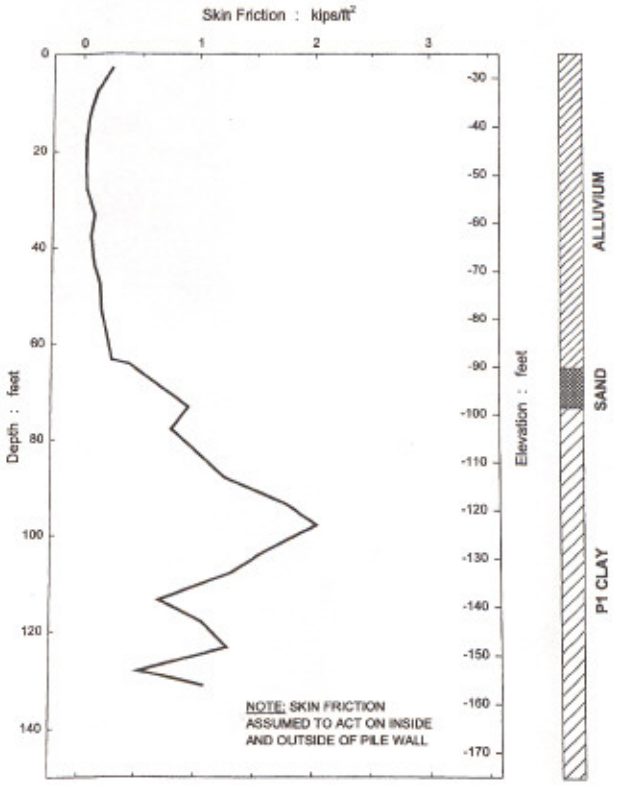

Fig. 6. Average skin friction during driving at location PL-1.

In these analyses, soil resistance was assumed to act on the steel annulus cross-sectional area of the pile (1.16 ft^2). The tip resistance was taken as 70 kips, computed using a unit end bearing of 60 ksf. This value was based partly on theoretical bearing capacity of the clay, and partly on relatively low tip resistance indicated by the CAPWAP analysis. The bearing capacity was computed from the undrained shear strength of the P1 clay, which was assessed as 8 ksf. Similar analyses were performed for the 42″ and 36″ pipe piles.

Pile Restrike Data

Most of the piles were redriven following a one-week and/or two-week rest period (Table 1). Figure 7 shows the end-of-driving and 14-day restrike soil resistances obtained from CAPWAP analyses of the monitoring data for the pipe piles. As expected, soil resistance increased with time after initial installation. The increases ranged from 12 to 60%, with the largest values for the all-clay profile (54″ piles at PL-1). It is unlikely that the force applied to the piles on the initial restrike blows was sufficient to fully mobilize the soil resistance. The data show that there is no relaxation of soil resistance in these soils, and that the end of driving soil resistances may be used in checking the production piles.

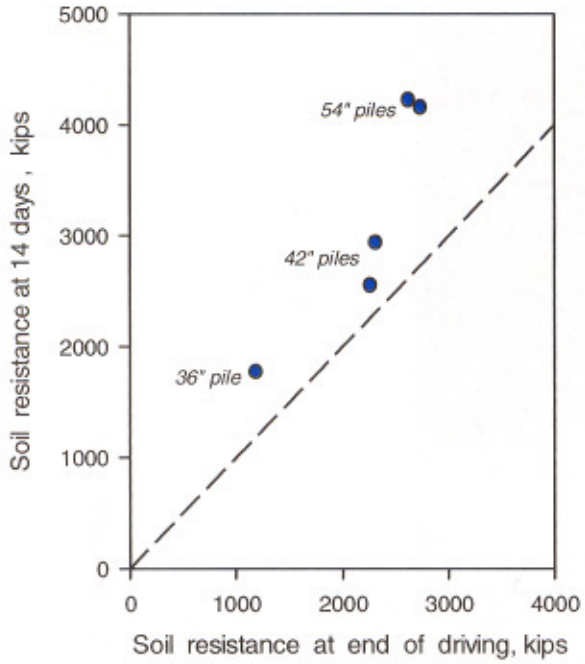

Fig. 7. Comparison of initial driving and 14-day restrike soil resistance from CAPWAP.

STATIC LOAD TEST RESULTS

Static pile load tests were performed several weeks after pile installation, conforming to ASTM D1143 on each pipe pile. The load test results for 54″ pipe pile C are shown on Figs 8 and 9 and summarized along with similar data for the other piles on Table 1.

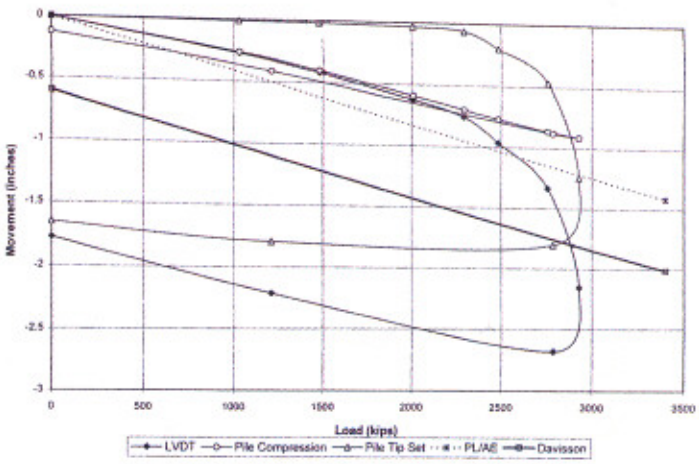

Fig. 8. Static load test at 54″ Pile C. Pile movement with load.

The relative tip resistances estimated from strain gauge measurements are indicative of plugged behavior, hence only the outside of the pile shaft would have participated in load transfer. The unit skin friction values shown on Fig. 9 were computed from the load transfer curves on this basis.

The test results indicate generally low total capacities for the pipe piles, considering the strength of the P1 clays and the P2 sands. The load transfer in the soils above the stronger sands and clays corresponds to skin friction values acting on the outside of the pile on the order of 0.8 ksf, which seems unrealistically high for these weak soils. Conversely, the load transfer in the P1 clay seems low, with skin friction values

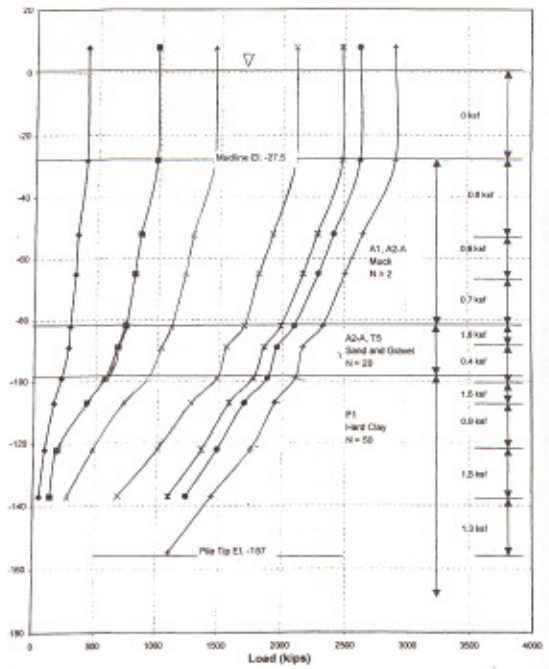

Fig. 9. Static load test at 54″ Pile C. Load distribution.

Table 3. Pile drivability with IHC S-280 hammer.

Pier	Pile Diameter (in)	Wall Thickness (in)	Ground Elev. (ft)	Planned Tip Elev. FS=1.9 (ft)	Blow Count at Tip Elev.	Driving Resistance (kips)	Planned Tip Elev. FS=2.25 (ft)	Blow Count at Tip Elev.	Driving Resistance (kips)	Elev. Reached at 300 bpf (ft)
V2	54	1"	5	-180	>300	4800	-205	>300	4800	-155
V2	54	11/4"	5	-180	300	5700	-205	>300	5700	-180
V2	54	11/4" to El -107, 1" below	5	-180	>300	5200	-205	>300	5200	-165
V1	72	1½" to El -117, 1" below	-35	-195	140	5500	-220	>300	6600	-190
V1	72	11/4" to El -117, 1" below	-35	-195	155	5500	-220	>300	6400	-215
M1	72	1½" to El -117, 1" below	-30	-215	300	6600	-240	>300	6600	-215
M1	72	11/4" to El -117, 1" below	-30	-215	>300	6400	-240	>300	6400	-210
M2	66	1½" to El -117, 1" below	-20	-175	70	4100	-200	135	5200	N/A
M3	66	1½" to El -117, 1" below	-3	-165	80	4300	-190	150	5400	N/A
M4	66	1"	-3	-160	100	4350	-185	250	5400	N/A
M5	54	1"	-3	-175	115	4000	-200	>300	4800	-190
M6	48	1"	-3	-150	180	4100	-180	>300	4400	-160
M7	48	1"	-3	-140	115	3800	-160	295	4400	N/A
M8	48	1"	-5	-150	180	4100	-170	>300	4400	-160
M8	48	7/8"	-5	-150	300	4100	-170	>300	4100	-150
M9	48	1"	-15	-150	115	3800	-170	295	4400	N/A
M10	48	1"	-10	-140	95	3600	-160	225	4250	N/A

Table 4. Pile drivability with IHC S-500 hammer.

Pier	Pile Diameter (in)	Wall Thickness (in)	Ground Elev. (ft)	Planned Tip Elev. FS=1.9 (ft)	Blow Count at Tip Elev.	Driving Resistance (kips)	Planned Tip Elev. FS=2.25 (ft)	Blow Count at Tip Elev.	Driving Resistance (kips)	Elev. Reached at 300 bpf (ft)
V2	54	1"	5	-180	>300	5300	-205	>300	5300	-170
V2	54	11/4"	5	-180	135	5700	-205	>300	6450	-200
V2	66	1"	5	-180	>300	6400	-205	>300	6400	-165
V1	72	1½" to El -117, 1" below	-35	-195	65	5500	-220	110	6600	N/A
V1	72	11/4" to El -117, 1" below	-35	-195	75	5500	-220	150	6600	N/A
M1	72	1½" to El -117, 1" below	-30	-215	110	6600	-240	280	7900	N/A
M1	72	11/4" to El -117, 1" below	-30	-215	150	6600	-240	>300	7600	-235
M2	66	1½" to El -117, 1" below	-20	-175	40	4100	-200	65	5200	N/A
M3	66	1½" to El -117, 1" below	-3	-165	45	4300	-190	70	5400	N/A
M4	66	1"	-3	-160	50	4350	-185	110	5400	N/A
M5	54	1"	-3	-175	60	4000	-200	160	5000	N/A
M6	48	1"	-3	-150	85	4100	-180	>300	4800	-175
M7	48	1"	-3	-140	55	3800	-160	130	4400	N/A
M8	48	1"	-5	-150	80	4100	-170	240	4750	N/A
M8	48	7/8"	-5	-150	160	4100	-170	>300	4350	-160
M9	48	1"	-15	-150	55	3800	-170	130	4400	N/A
M10	48	1"	-10	-140	50	3600	-160	105	4250	N/A

between 0.9 and 2.3 ksf. The P1 clay is heavily over consolidated, with undrained shear strength on the order of 7 to 8 ksf. The published database of load tests on pipe piles would indicate skin friction values on the order of 3 to 4 ksf.

The tip resistance of about 1,000 kips acting on the 54″ pipe pile (Fig. 9) is about one-third of the total axial capacity of the pile. The magnitude of the tip resistance confirms expectations that the pile behaved as plugged under static loading conditions. The tip resistance corresponds to a unit end bearing value of 63 ksf on the gross end area of the pile. The undrained shear strength of the P1 clay may then be estimated as about 7 ksf, assuming a conventional bearing capacity factor of 9.

Parameters for Axial Load Capacity

Unit skin friction and end bearing parameters were established based on field and laboratory tests and on engineering judgment to derive design axial pile load capacity. The weak upper soils were not considered as contributing to the capacity, as the alluvium is considered to be removed by scour, and the fill was ignored. Based on the static pile load test program, an average ultimate unit skin friction of 1.7 ksf was selected for the stronger sands and clays beneath the fill and/or alluvium. The piles were considered plugged, with skin friction acting on the exterior of the pile. Ultimate end bearing was taken as 63 ksf, acting over the gross end area of the pile.

The above parameters were used for larger diameter piles up to d = 72″ at the bridge site. The foundation piles will need to penetrate to greater depths than tested in the pile demonstration program, due to use of fewer piles and higher loads in the final design.

PREDICTED PILE DRIVEABILITY

The parameters for axial load capacity given above were used to determine the required tip penetrations for the production piles. The required penetrations are given on Tables 3 and 4, and have values that vary depending on the factor of safety applied. The primary purpose of Tables 3 and 4 is to indicate the predicted pile driveability for IHC S-280 and S-500 hammers. The driving resistance is soil resistance computed by wave equation analyses for various foundation piles using the parameters on Table 2. Note that driving resistance is also affected by the pile stiffness. The refusal criterion for these hydraulic hammers, taken as 300 bpf, is exceeded by some of the pile-hammer combinations.

The required safety factor (SF) based on AASHTO specifications, depends on the level of testing performed for quality assurance. Use of SF = 1.9 assumes static pile load testing is performed on production piles at the time of construction. Without such testing, the required SF = 2.25.

The largest shortfall in pile penetration is for Pier V2, which is unique in having a predicted scour potential that removes a portion of the stronger soils (mainly P2 sands) as well as the weaker overlying materials (see Fig. 3). Consequently, the difference between static pile capacity and soil resistance at the time of pile driving is greater for Pier V2 than for the other bridge piers. This difference between the existing ground conditions and the maximum scour design condition must be considered when comparing pile driving performance with target static capacity of the piles.

SEISMIC SOIL-STRUCTURE INTERACTION

Recognizing the importance of the bridge and the consequences of a potential damaging earthquake, seismic issues were addressed throughout the new design to ensure acceptable performance, although the seismicity of the area is low. Design events with return period of 500 and 2,500 years were examined. Three-dimensional dynamic soil-foundation interaction analyses were performed to examine effects of site conditions and pile foundations on design seismic motions.

Free-Field Ground Motions

The soil profile along the longitudinal axis of the bridge is shown on Fig. 3. Bedrock is 500 to 700 ft below sea level. A site-specific ground motion analysis was performed by URS Corporation, utilizing the seismicity of the region and the soil conditions. Uniform hazard rock spectra for 2,500-year return period were established following a probabilistic seismic hazard analysis approach, incorporating regional seismicity data and attenuation laws applicable to the eastern United States (US). Figure 8 shows the resulting horizontal and vertical design rock spectra. An 85% confidence interval was selected to account for all parametric uncertainties and subjective judgment.

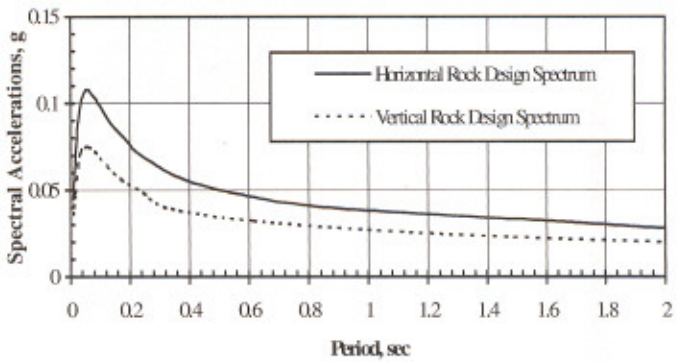

Fig. 8. Horizontal and vertical uniform hazard rock spectra for 2500-year return period.

Site specific, spectrum-compatible rock input motions were developed, using typical rock records appropriate for seismic analysis in the eastern US. The selected records were adjusted so that their spectra matched reasonably well the uniform hazard rock spectrum for the horizontal direction, as shown in Fig. 8. The computer program SHAKE was then used to

establish amplification characteristics of various soil columns that represented site conditions along the bridge. The resulting amplification ratios were used to adjust the rock spectra and establish free-field soil spectra for the regions investigated.

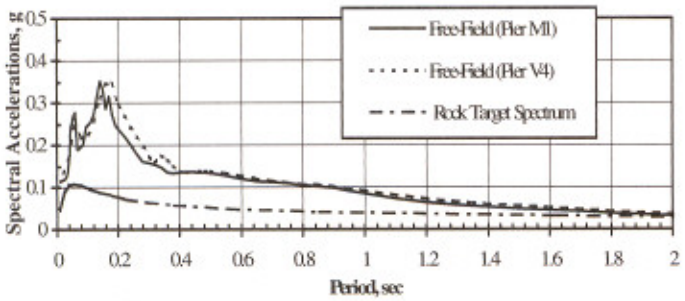

Fig. 9. Computed free-field ground surface spectra for pier locations M1 and V4.

Finally, using these design ground motion spectra as targets, free-field acceleration time histories were generated having response spectra very closely matching the target spectra of the different regions.

Figure 9 shows the spectra of the generated free-field ground motions for two typical locations: the bascule span region (Pier M1) where 25 ft of scour is included, and the location of Pier V4 where the pile cap is in the ground, and scour is not an issue. The free-field ground motions were subsequently used in the soil-foundation interaction analysis to generate the foundation (cap-base) motions needed in the soil-structure interaction (SSI) analysis of the bridge.

Soil-Foundation Interaction Analyses

The pier foundations are quite different due to significant variability in soil conditions and scour predictions along the bridge. The piers over the river are founded on frictional and partially bearing steel pipe piles that are as much as 30 ft above mudline, with long laterally unsupported lengths. Figure 10 shows the foundation details of pier M1.

Five of the prestressed concrete piles in the piers on the Virginia side are founded on land with no scour concern. The foundation of a typical pier (V4) is shown on Fig. 11. In this region, the pile cap will be about 10 ft below ground surface.

The potential scour in the river channel is high (50 ft). Under seismic conditions, scour is taken into account by considering one case with 50% of full scour and another with no scour at all. Full scour conditions were examined under service conditions, i.e., dead and live loads. For the superstructure, which is supported on lead core rubber bearings, "no scour" conditions generally controlled.

During a seismic event, ground motions propagating through the foundation soils will transmit energy through the piles to the bridge superstructure. In turn, the resulting inertial forces from the bridge will be transmitted to the soil through the pile foundation. This soil-structure interaction (SSI) was modeled through foundation springs placed at the base of the pile caps as shown schematically in Fig. 12.

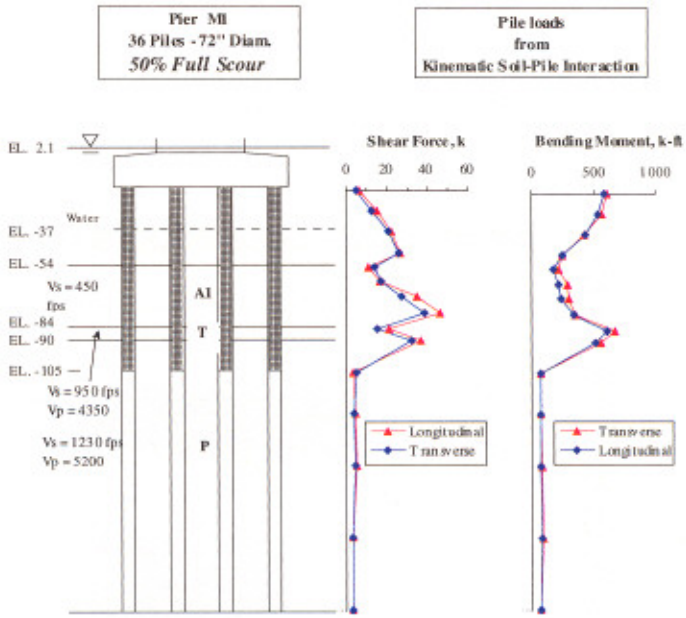

Fig. 10. Soil and foundation details for bascule Pier M1, and results of 3-D SSI analysis.

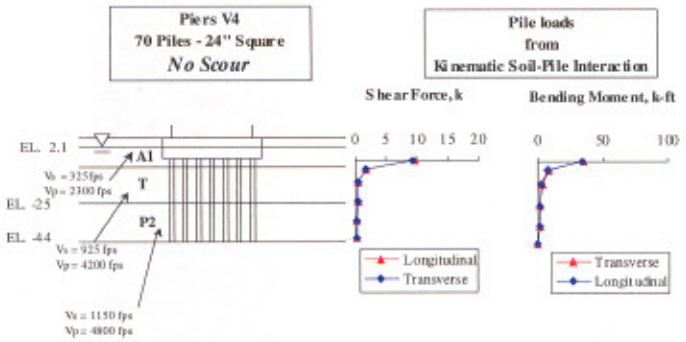

Fig. 11. Soil and foundation details for bascule Pier V4, and results of 3-D SSI analysis.

Due to large unsupported length of the channel piers, the motion at the pile cap level can be significantly different from the free-field ground surface motion, resulting to large spectral accelerations, especially in the fundamental period of the pile-soil system. The shear forces and bending moments induced by these ground motions and pile inertia are in addition to the inertial loads from the superstructure and were accounted through soil-foundation interaction analyses. The calculated pile cap-base motions (E-cap-base) were then specified as the input in the overall SSI bridge analysis, as shown in Fig. 12.

The first part of the seismic soil-foundation interaction analysis involved calculation of the cap-base motions using the free-field motions. The second part was to compute pile

shear forces and bending moments induced by both seismic waves (kinematic effect) and pile inertia. Finally, foundation stiffness coefficients were calculated for use in the SSI analysis of the superstructure. The following subsections describe these three analyses and present the results.

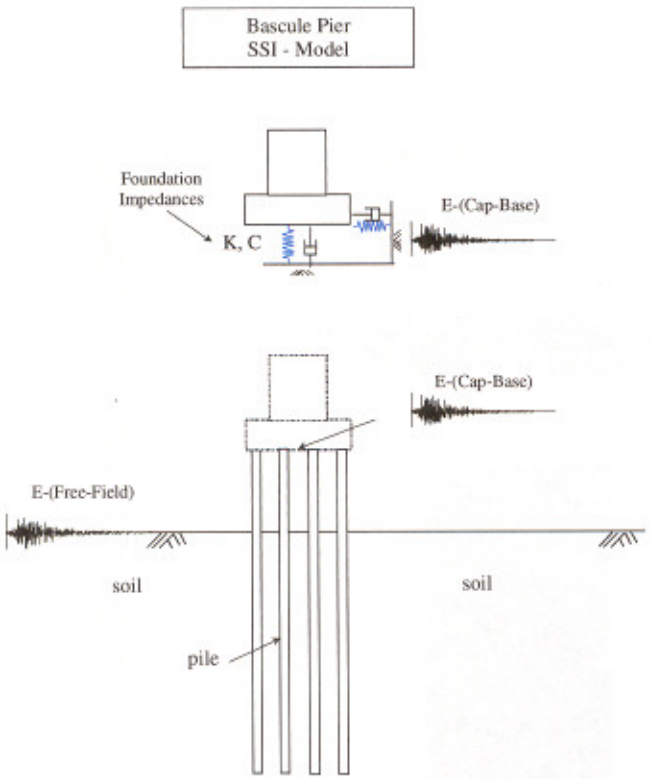

Fig. 12. Soil-foundation interaction and foundation-bridge interaction models used in the bridge seismic analysis.

Cap-Base Motions

To compute earthquake motions at the top of the piles (bottom of the massless caps), 3-D seismic soil-foundation interaction analyses were performed using the computer program SASSI (ACS, 1998). The program utilizes the finite element method with transmitting boundaries to model deformations and dissipation of energy away from the finite element mesh boundaries.

Figure 13 shows SASSI models of the bascule foundation M1 (Fig. 10) and Virginia foundation V4 (Fig. 11). Solid elements were used to model the soil and concrete cap, and beam elements were used to model the piles. The site-specific free-field motions were used as input at the ground surface. In the SASSI analysis, soil behavior is assumed to be linear and governed by the soil shear wave velocity. However, it is well recognized that soils exhibit nonlinear stress-strain behavior. Seismic waves propagating though a soil profile in absence of the structure and its foundation generate shear strains that lead to reduction in the soil modulus. This effect was accounted approximately in the SASSI analysis by using reduced, strain-dependent shear wave velocities as computed in the free-field ground motion SHAKE analyses (shown in Figs 10 and 11).

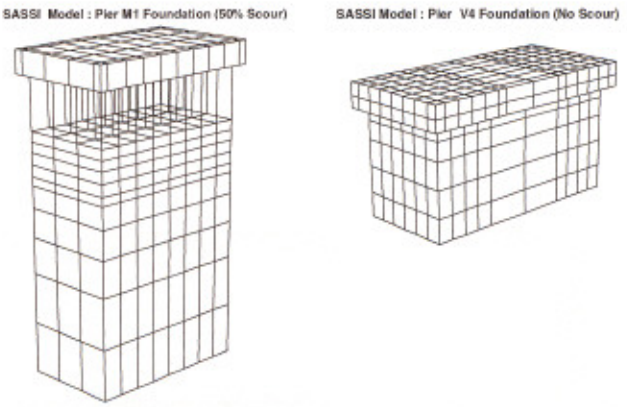

Fig. 13. SASSI models used for pier foundations M1 and V4.

Figure 14 shows free-field ground surface spectrum at pier M1 and the spectrum at the base of the cap in the longitudinal direction. Since the horizontal free-field ground motions were the same in longitudinal and transverse directions, and the pile caps were symmetric about these two axes, the differences in the cap-base spectra for the two directions were insignificant.

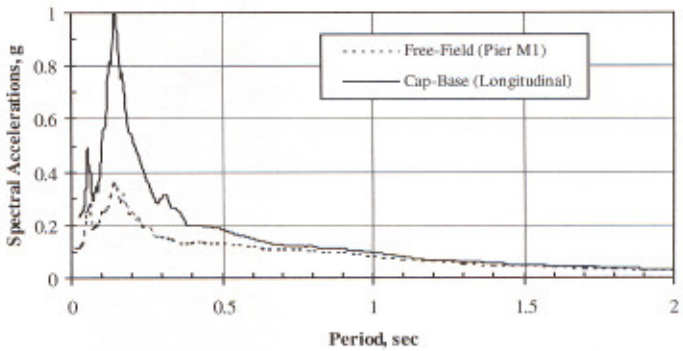

Fig. 14. Comparison of cap-base and surface free-field motion response spectra at Pier M1.

FOUNDATION OPTIMIZATION

Using results from the Pile Demonstration Program, Wave Equation Analyses and driveability studies, alternative pile arrangements were investigated considering varying pile diameter, wall thickness and pile spacing. Required pile tip elevations were determined based on ultimate capacities and compared with the predicted driveability tables to verify that the piles could achieve the required tip elevation.

Table 5 shows a summary of alternative foundations investigated at each pier. It can be seen that the larger diameter, higher capacity piles produce the more cost effective designs. It was also recognized that field splicing of large diameter, heavy wall pipes would be extremely costly and time consuming. Therefore it was desirable to install these

Table 5. Foundation optimization. Recommended foundations are shown in bold.

PIER	LAYOUT		PERFORMANCE		PILE DATA		OBTAINABLE S500 (369 ft-k) HAMMER		WEIGHT	PILES REDUCTION (with resp. to reference)	COST OF PILES	RIG DAYS TO INSTALL PILES
	Piles	Pile Cap	Biaxial Unity Check	AASHTO Group	TIP ELEV. (ft)	Req'd CAPACITY Qu (kips)	TIP ELEV. (ft)	Predicted Blows (b/ft)	Single Pile (tons)			
V3 to V5	2x24 - 36" - 3/4"	2x(46.5' x 31.5')	0.776	I	-110	2122			21	REF.	$3,125,500	24
	2x20 - 36" - 3/4"	2x(45' x 31.5')	0.941	I	-125	2595			16	32	$2,945,800	20
	2x20 - 36" - 3/4"	2x(46.5' x 31.5')	0.905	I	-125	2544			26	32	$2,945,800	20
	2x14 - 36" - 1"	2x(45' x 27')	0.867	I	-145	3382			27	80		
	2x14 - 42" - 7/8"	2x(45' x 27')	0.866	I	-130	3399			25	80		
	2x60 - 24"sq conc	2x(53' x 33')		I	-30	883			7	-288	$1,088,000	60
	2x35 - 24"sq conc	**2 x (44' x 32')**		**I**	**-44**	**1462**			**12**	**-68**	**$999,000**	**53**
V6 / V7	2x24 - 36" - 3/4"	2x 46.5' x 31.5'	0.776	I	-110	2122			21	REF.	$4,697,200	36
	2x20 - 36" - 3/4"	2x 45' x 31.5'	0.941	I	-120	2595			16	48	4,256,300	30
	2x20 - 36" - 3/4"	2x 46.5' x 31.5'	0.905	I	-120	2544			26	48	4,256,300	30
	2x14 - 36" - 1"	2x 45' x 27'	0.867	I	-140	3382			27	120		
	2x14 - 42" - 7/8"	2x 45' x 27'	0.866	I	-130	3399			25	120	4,300,100	21
	2x60 - 24"sq conc	53' x 33'		I	-30	883			7	-432	1,622,000	90
	2x30 - 24"sq conc	**2 x 44' x 32'**		**I**	**-44**	**1184**			**12**	**-48**	**$668,200**	**35**
V2	2x24 - 42" - 1"	2x 53.5' x 35.75'	0.742	III	-120	2056			26	REF.	3,253,500	96
	2x20 - 42" - 1 1/4"	2x 51.5' x 35.75'	0.863	III	-140	2645			33	16	3,622,650	80
	2x12 - 48" - 1 1/2"	2x 53.25' x 39.5'	1.030	I	-280	4676			100	48	5,091,900	130
	2x15 - 54" - 1"	**2 x 60' x 39.5'**	**0.947**	**I**	**-205**	**3455**	**-170**	**300**	**61**	**18**	**$5,145,550**	**60**
V1 / M1	2x35 - 54" - 1 1/4"	2x 78' x 55.5'	0.544	VIII	-135	2382			49	0	22,669,900	140
	2x20 - 66" - 1 1/2"	2x 77.5' x 52.75'	0.502	VIII	-145	3843			72	120	21,290,200	107
	2x18 - 72" - 1 1/2"	2x 72' x 57'	0.561	VIII	-145	4270			79	136	22,364,950	144
	2x12 - 66" - 2"	2x 66' x 48'	0.710	VIII	-190	6236			146	184		
	2x10 - 72" - 1 7/8"	2x 66' x 48'	0.760	VIII	-227	7545			160	200		
	2x24 - 54" - 1 1/4"	2x 78' x 51'	0.810	VIII	-155	3234			65	88		
	2x10 - 66" - 2"	2x 66' x 48'	0.905	VIII	-227	7545			171	200		
	2x8 - 72" - 2 7/8"	2x 60' x 52'	0.905	VIII	-230	9641			293	216		
	36 - 72" - 1 1/2"	**128.5' x 78'**		**VII**	**-200**	**4356**	**-210**	**90**	**100**	**136**	**$14,807,550**	**72**
M2	2x24 - 54" - 1 1/4"	2x 66.75' x 44.25'	0.914	VESSEL	-130	2114			46	REF.	6,767,400	48
	2x12 - 66" - 1 3/4"	2x 66' x 48'	0.929	VESSEL	-130	3711			67	96	7,096,350	32
	2x10 - 72" - 1 3/4"	2x 66' x 48'	0.885	VESSEL	-130	4138			73	112	6,571,950	40
	2x8 - 66" - 1 1/4"	2x 60' x 44'	0.870	VESSEL	-249	8054			170	144		
	2x7 - 66" - 1 1/4"	2x 54' x 44'	0.820	VESSEL	-241	7734			165	136	4,386,350	19
	2x12 - 66" - 1 1/2"	**2 x 53.25' x 39.5'**	**0.936**	**VESSEL**	**-195**	**4060**	**-195**	**65**	**88**	**96**	**$8,323,000**	**32**
M3	2x24 - 54" - 1 1/4"	2x 66.75' x 44.25'	0.590	VIII	-130	2114			46	REF.	6,343,550	48
	2x12 - 66" - 1 3/4"	2x 66' x 48'	0.790	VIII	-130	3711			67	96	6,164,650	32
	2x12 - 66" - 1 1/4"	2x 53.25' x 39.5'	0.794	VIII	-130	3758			67	96	4,696,150	32
	2x10 - 72" - 1 3/4"	2x 66' x 48'	0.494	VIII	-130	4138			73	112	6,606,250	40
	2x6 - 66" - 1 1/4"	2x 60' x 44'	0.550	VIII	-249	8054			170	144		
	2x7 - 66" - 1 1/4"	2x 54' x 44'	0.520	VIII	-241	7734			165	136	4,216,850	19
	2x12 - 66" - 1 1/2"	**2 x 53.25' x 39.5'**	**0.851**	**VESSEL**	**-190**	**4048**	**-190**	**70**	**88**	**96**	**$8,137,000**	**32**
M4/M5	2x24 - 42" - 1"	2x 53.25' x 39.75'	0.593	VIII	-125	1731			27	REF.	6,600,200	64
	2x15 - 42" - 1"	2x 51.5' x 30.5'	0.834	VIII	-160	2883			27	108		
	2x13 - 54" - 3/4"	2x 51.5' x 30.5'	0.807	VIII	-135	3145			27	132	5,371,800	52
	2x12 - 66" - 1 1/4"	2x 53.25' x 39.5'	0.655	VIII	-135	3932			27	144	11,174,450	64
	2x10 - 72" - 1.5"	2x 57' x 42'	0.544	VIII	-130	4404			27	168	10,859,050	80
	2x12 - 54" - 1"	2x 44.25' x 33'	0.645	VIII	-155	3942			27	144		
	2x12 - 54" - 1"	2x 53.25' x 39.5'	0.705	VIII	-115	3298			27	144	6,158,100	48
M4	**2x12 - 66" - 1"**	**2 x 53.25' x 39.5'**	**0.919**	**I**	**-185**	**3861**	**-185**	**110**	**68**	**144**	**$5,691,650**	**32**
M5	**2x12 - 54" - 1"**	**2 x 53.25' x 39.5'**	**0.761**	**VIII**	**-200**	**3584**	**-195**	**300**	**60**	**144**	**$4,169,000**	**24**
M6	2x24 - 42" - 1"	2x 53.25' x 39.75'	0.505	VIII	-90	1474			27	REF.	2,499,400	32
	2x15 - 42" - 1"	2x 51.5' x 30.5'	0.712	VIII	-120	2461			27	108	1,975,950	20
	2x12 - 42" - 1.25"	2x 36.75' x 28'	0.780	VIII	-150	3845			27	108		
	2x13 - 54" - 3/4"	2x 51.5' x 30.5'	0.689	VIII	-95	2685			27	132	2,530,500	26
	2x12 - 54" - 1"	2x 53.25' x 39.5'	0.705	VIII	-115	3298			27	132	3,111,800	24
	2x12 - 66" - 1 1/4"	2x 53.25' x 39.5'	0.655	VIII	-105	3932			27	144	3,814,100	32
	2x10 - 72" - 1.5"	2x 57' x 42'	0.544	VIII	-105	3743			27	168	2,658,325	40
	2x12 - 48" - 1"	**2 x 53.25' x 39.5'**	**0.844**	**VIII**	**-180**	**3264**	**-170**	**300**	**48**	**132**	**$2,506,650**	**16**
M7 to M10	2x24 - 42" - 1"	2x 53.25' x 39.75'	0.485	VIII	-80	1416			22	REF.	9,178,450	128
	2x15 - 42" - 1"	2x 51.5' x 30.5'	0.683	VIII	-105	2361			22	144	7,069,000	80
	2x12 - 42" - 1"	2x 36.75' x 28'	0.963	VIII	-120	3072			22	144		140
	2x12 - 54" - 3/4"	2x 53.25' X 39.5'	0.737	VIII	-95	2768			22		6,850,900	96
	2x13 - 54" - 3/4"	2x 51.5' x 30.5'	0.661	VIII	-85	2576			22	132	7,418,150	104
	2x12 - 66" - 1 1/4"	2x 53.25' x 39.5'	0.546	VIII	-85	3277			22	144	8,186,300	128
	2x10 - 72" - 1.5"	2x 57' x 42'	0.453	VIII	-80	3670			22	168	14,219,800	160
	2x10 - 48" - 1"	**2 x 40' x 30'**	**0.928**	**VIII**	**-200**	**3436**	**-180**	**300**	**53**	**168**	**8,889,300**	**54**

piles in one piece which afforded better quality control during fabrication. The weight of the piles were calculated and compared with the lifting capacities of the rigs anticipated for use on the project as well as the necessary lifting radii.

PRODUCTION QUALITY CONTROL

Pile monitoring will be performed during production pile installation. Figure 4 shows the increase in soil resistance during initial driving of the 54″ piles, as indicated by PDA results and CAPWAP analysis. Also shown on Fig. 4 is the static capacity obtained from the load test on pile C. The trend lines of soil resistance during driving indicate similar values to the static load test result.

Figure 15 compares PDA soil resistances at the time of driving during initial installation of the demonstration program pipe piles and the subsequent ASTM D-1143 static pile capacity measurements. The static capacity plotted for the 42″ pile is noted to be a lower bound to the actual static capacity. The pile did not reach failure under the maximum static load of 2,000 kips (see 42″ pile data points on Fig. 15). There is a reasonably close correspondence between PDA soil resistance and static capacity. However, the agreement is improved if the soil resistance is increased by adding 200 kips to the PDA values. This appears to provide a convenient and appropriate means of estimating the static capacity of the piles, based on measurements made during their installation.

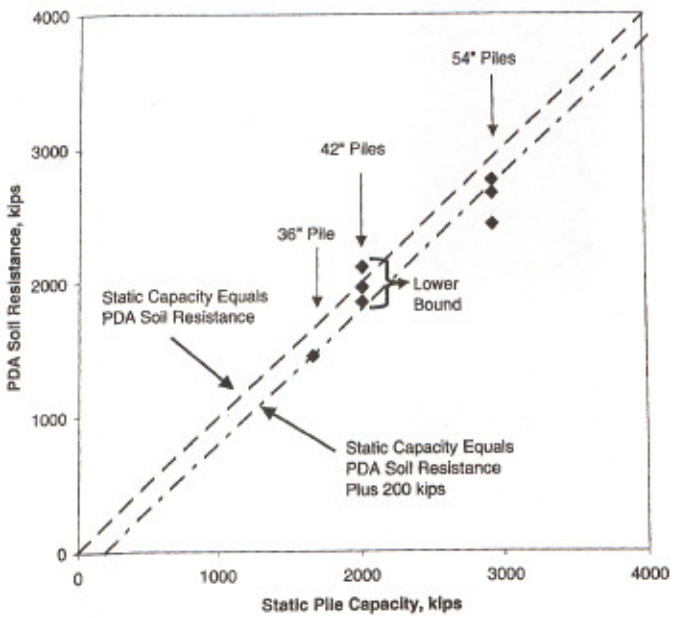

Fig. 15. Comparison of static capacity and PDA soil resistance for 36″, 42″, and 54″ pipe piles.

As discussed earlier, the design scour condition is predicted to remove some of the stronger soils from beneath Pier V2. Specifically, the design scour level El -76 corresponds to the removal of some 45 ft of the stronger soils from around the pile shafts. The piles will need to be driven in current soil conditions to a capacity greater than the design capacity. The ratio of static capacities for current and design (maximum scour) soil conditions depends on pile diameter and planned pile penetration. This should be determined in detail once the pile size and planned pile penetrations (i.e., target safety factors) are finalized. As a guide, the required static capacities for current soil condition at pier V2 are about 30% greater than the design, fully scoured, capacities. The required static capacity for the current conditions instead of design capacities were used when implementing production quality control.

PILE ACCEPTANCE CRITERIA

In absence of load testing during construction, the required pile penetrations have been conservatively established using a 2.25 factor of safety on the most heavily loaded piles. Driveability studies predict high to near refusal driving resistance with the larger of the two hammers evaluated. Piles achieving the estimated tip elevation and driving resistance were considered acceptable. Piles not reaching the estimated tip elevation can be re-evaluated in the field considering the actual pile loads, including their statistical distribution, and indicated PDA soil resistance.

CONCLUSIONS

The ability to perform design phase testing enabled the designers to optimize the foundations for the new Woodrow Wilson Memorial Bridge, resulting in significant cost savings for the project. State of the art seismic modeling techniques allowed for more precise evaluation of the overall structural performance and response under varying load combinations and soil conditions. Simplified installation using specified tip elevation and elimination of static load tests during construction, in combination with dynamic testing facilitated quality assurance and control during construction and allowed for quick response and remedial action in the field.

ACKNOWLEDGMENTS

The new Woodrow Wilson Bridge is a joint project of Federal Highway Administration (FHWA), Maryland State Highway Administration (MSHA), and Virginia Department of Transportation (VDOT).

The project was designed and managed by Parsons Transportation Group PTG). The contribution of Dr. Serafim G. Arzoumanidis of PTG, Project Manager for the new bridge, was instrumental in establishing the overall design approach and coordinating all team members.

Other consultants involved in the geotechnical and seismic aspects of the project were:

- Potomac Crossing Consultants (Parsons Brinkerhoff, URS Greiner & Rummel, Klepper & Kahl) performed geotechnical investigations and pile demonstration program.
- McLean Contracting Company performed the pile demonstration program.
- D.W. Kozera, Inc. performed Static load testing, PDA monitoring and CAPWAP analyses (as subcontractor to McLean).
- Applied Foundation Testing, Inc. performed Statnamic load tests on piles B and E (as subcontractor to McLean)

REFERENCES

ACS-SASSI-C [1998]. An advanced computational software for 3D Structural Analysis including Soil-Structure Interaction, ACS, Inc., Pittsford, New York.

American Society of Testing and Materials [1994]. ASTM D-1143-81: Standard Test Method for Piles under Static Axial Compressive Loads

American Society of Testing and Materials [1995]. ASTM D-3966-90: Standard Test Method for Piles under Lateral Loads

Applied Foundation Testing, Inc. [2000]. "Axial Statnamic Load Testing, Woodrow Wilson Bridge Load Test Program," August 30

CAPWAP [1998]. CAse Pile Wave Analysis Program, Goble Rausche Likins and Associates, Inc., Cleveland, Ohio

Dutt & Collins [1995]. "A Simple Model to Predict Soil Resistance to Driving for Long Piles in Deepwater Normally Consolidated Clays," *Offshore Technology Conference, Houston*, 257-269

Ellman, R.A., Jr. [2002]. Invited Presentation to *ASCE GEOInstitute International Deep Foundations Congress*

FLPIER [2001]. Nonlinear finite element software for analysis of bridge pier structures, Bridge Software Institute, University of Florida (written by Hoit, Mc Vay & Hays)

Geosciences Testing & Research, Inc. [2000]. "Pile Foundation Capacity - Dynamic Analysis, Federal Aid Project No. FAP-DPWW-013(11)N, Woodrow Wilson Bridge Pile Load Test Program," October 3

Kozera, D.W., Inc. [2000]. "Dynamic Pile Monitoring of Piles, Pile Demonstration Program, Woodrow Wilson Bridge Replacement, I-95 over the Potomac River, MD," August 28

Mueser Rutledge Consulting Engineers [2000]. "Woodrow Wilson Memorial Bridge, Final Review Submission, Contract 2 – Foundations," July 31

Nikolaou, S., Mylonakis, G., Gazetas, G., & Tazoh, T. [2001]. "Kinematic Pile Bending During Earthquakes: Analysis and Measurements," *Geotechnique*, 51(5):425-440

Reese, Cox, & Koop [1974]. "Analysis of Laterally Loaded Piles in Sand," *5th Offshore Technology Conference*, Houston, Paper No. 2080

Schnabel, B., Lysmer, J., & Seed, B.H. [1972]. SHAKE91: A computer program for conducting equivalent linear seismic response analyses of horizontally layered soil deposits. *Report No. EERC 72-12, University of California, Berkeley*, modified by Idriss & Sun (1991).

Stevens, Wiltsie, & Turton [1982] "Evaluating Driveability in Hard Clay, Very Dense Sand, & Rock," *Offshore Technology Conference*, Houston, 465-469

Yegian, M.K., Arzoumanidis, S., Nikolaou, S., & Cooling T. [2002]. "Seismic Soil-Foundation Interaction Analyses of the New Woodrow Wilson Bridge," *7th US Conference on Earthquake Engineering*, Boston, July 21-25